Acta Pharmaceutica Sinica B 2021;11(1):246–257

Chinese Pharmaceutical Association
Institute of Materia Medica, Chinese Academy of Medical Sciences

Acta Pharmaceutica Sinica B

www.elsevier.com/locate/apsb
www.sciencedirect.com

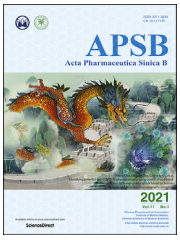

ORIGINAL ARTICLE

A smart dual-drug nanosystem based on co-assembly of plant and food-derived natural products for synergistic HCC immunotherapy

Bingchen Zhang[a,†], Jiali Jiang[a,†], Pengyu Wu[a], Junjie Zou[a], Jingqing Le[a], Juanfang Lin[a], Chao Li[a], Bangyue Luo[a], Yongjie Zhang[a], Rui Huang[b], Jingwei Shao[a,b,*]

[a]*Fujian Provincial Key Laboratory of Cancer Metastasis Chemoprevention and Chemotherapy, College of Chemistry, Fuzhou University, Fuzhou 350116, China*
[b]*Institute of Oceanography, Minjiang University, Fuzhou 350108, China*

Received 11 July 2020; received in revised form 31 August 2020; accepted 10 September 2020

KEY WORDS

Natural product;
Ursolic acid;
EGCG;
Aptamer;
Co-assembly;
Nanodrug;
HCC;
Synergistic treatment;
Immunotherapy

Abstract Nanotechnology has emerged as an ideal approach for achieving the efficient chemo agent delivery. However, the potential toxicity and unclear internal metabolism of most nano-carriers was still a major obstacle for the clinical application. Herein, a novel "core–shell" co-assembly carrier-free nanosystem was constructed based on natural sources of ursolic acid (UA) and polyphenol (EGCG) with the EpCAM-aptamer modification for hepatocellular carcinoma (HCC) synergistic treatment. As the nature products derived from food-plant, UA and EGCG had good anticancer activities and low toxicity. With the simple and "green" method, the nanodrugs had the advantages of good stability, pH-responsive and strong penetration of tumor tissues, which was expected to increase tumor cellular uptake, long circulation and effectively avoid the potential defects of traditional carriers. The nanocomplex exhibited the low cytotoxicity in the normal cells *in vitro,* good biosafety of organic tissues and efficient tumor accumulation *in vivo*. Importantly, UA combined with EGCG showed the immunotherapy by activating the innate immunity and acquired immunity resulting in significant synergistic therapeutic effect. The research could provide new ideas for the research and development of self-assembly delivery system in the future, and offer effective intervention strategies for clinical HCC treatment.

*Corresponding author.
E-mail address: shaojw12@163.com (Jingwei Shao).
[†]These authors made equal contributions to this work.
Peer review under responsibility of Institute of Materia Medica, Chinese Academy of Medical Sciences and Chinese Pharmaceutical Association.

https://doi.org/10.1016/j.apsb.2020.07.026

1. Introduction

Primary liver cancer is one of the most intractable malignant diseases throughout the world, which remains the second cancer death of about 841,000 newly diagnosed cases and 782,000 deaths annually[1]. Hepatocellular carcinoma (HCC), accounting for about 80% of primary liver cancer, still displays an increasing morbidity and mortality rates[2]. In the past few decades, HCC survival has little discernible improvement in most countries because the majority of patients were diagnosed at an advanced stage[3]. Moreover, outcomes of surgical and chemical treatment are overall disappointed[4,5]. Conventional chemotherapy agents, such as doxorubicin, cisplatin or mitomycin C, still confronted with problems like low bioavailability, poor objective response rate and inevitably acquired resistance[6]. In recent years, significant progress in the research on drug delivery systems has been achieved along with advances in pharmaceutical sciences[7]. With the valuable research in the field of drug delivery, the development of safer and more effective drugs or combination therapy project for advanced HCC is in urgent need.

Ursolic acid (UA) is a pentacyclic triterpene compound which has been confirmed to possess anti-metastatic, anti-angiogenic, anti-inflammatory and anti-proliferative potential through extensively studying *in vitro* and *in vivo* models of cancer[8,9]. Additionally, as a natural product, UA has the advantages of low toxicity and high efficacy compared with conventional chemotherapy agents, which has attracted increasing interest into scientists over the past few decades[10]. However, the poor water solubility of UA still limits its application as other chemo agents[11]. The nanoscale drug delivery system, such as mesoporous silica, liposome and dendrimer, could greatly enhance the UA permeability, promote cellular uptake, and improve poor bioavailability *in vivo*[12−14]. Nevertheless, low drug-loading as well as potential toxicity are prominent obstacles of nano-carriers[15].

Recently, the "carrier-free" nano-drug delivery system comes up to be a new strategy to address the above mentioned problems[16]. In our previous study, we also synthesized a series of carrier-free nanoparticles to solve the problem of traditional nano-carrier. We demonstrated that UA could be a carrier-free nanodrug by self-assembly, which exhibited effective HCC therapy[17]. On this base, we also showed that the combination of old drugs (aspirin), or chemo agent (doxorubicin) with UA to establish a self-assembly dual-nanodrug for synergistic cancer treatment, which can either promote inhibitory efficiency of proliferation, metastasis or improve drug bioavailability[18,19]. Very recently, we have also successfully developed a co-assembly of UA and photosensitizer of ICG for cancer imaging and chemo−photo combination therapy[20].

With these achievements and information, we started to conceive to develop the more stable and "green" treatment formulation. Epigallocatechin gallate (EGCG), the most abundant ingredient in green tea, which is a well-known beverage for its antioxidant and cardiovascular protected abilities[21,22]. Meanwhile, anti-cancer effect of EGCG has been demonstrated, such as inhibition of cancer cells proliferation, migration, invasion and metastasis, etc[23,24]. Recently, EGCG was reported as "shell" for the coating of multifunctional materials. It could self-polymerize to form a uniform layer for generating coatings on a variety of organic and inorganic substrates at alkaline pH values to avoid the degradation of "core"[25,26]. Taking the results of these exploratory research into consideration, as well as the fact that the trihydroxyphenyl functional group and the strong solid–liquid interfacial activity were the common feature of EGCG, ECG, and other plant polyphenols, it could be one of the reasons that EGCG formed a coating by strongly binding to surfaces through non-covalent interactions. In addition, the oxidation reaction was also responsible for the formation of coatings from ECGC, which inspired coatings form spontaneously at mildly alkaline pH in the presence of available dissolved oxygen, likely through phenolate ion intermediaries[26]. Futhermore, imputing to existence of galloyl and catechol groups, EGCG enabled the noncovalent interaction with various biological molecules, such as DNA and RNA[27].

Aptamer (Apt) were synthetic single nucleic acid chains that could specifically bind to various targets through molecular recognition[28]. The main merits of Apt should be their size, synthetic accessibility, high affinity, increased stability, and lack of immunogenicity[29,30]. Epithelial cell adhesion molecule (EpCAM) was chosen for the Apt targeting as a trans-membrane glycoprotein that played roles in tumor cell migration, proliferation and differentiation[31,32]. By modifying the EpCAM-Apt on the "shell" of EGCG, the targeting effect of self-assembly NPs could be significantly enhanced for EpCAM-positive cells, which have been illustrated to be in charge of HCC growth and invasiveness[33].

In this work, a carrier-free, self-assembly nanodrugs based on UA and EGCG modified by EpCAM-aptamer was developed for targeted HCC treatment (Fig. 1A). UA had the advantage of liver protection and efficient tumor growth inhibition made it suitable for HCC treatment[34]. Meanwhile, UA could be prepared as the nanoscale drug by the unique phenomenon of self-assembly. EGCG coating in the surface of UA NPs aims to form "core–shell" nanostructure, which enhanced stability of NPs and promoted targeting ability by binding aptamer. In addition, EGCG could easily be biodegraded by acidic pH, leading to increased drug release in tumor tissues so as to enhance anti-cancer capacity[35]. It is noteworthy that EGCG had the similar immunostimulatory with UA, which was recognized to remarkably activate innate immunity and significantly increase T cells frequencies and numbers in spleen and lymph nodes[36,37]. We hypothesized that UA in nanosystem could not only cause the tumor cells death and provide tumor antigens, but combine with EGCG activate natural immunity and enhance APC cell proliferation at the same time, so as to realize the further clearance of tumor by acquired immune cells (Fig. 1B). Compared with traditional nano-carriers, the preparation of self-assembly NPs was more likely to reduce side effects, such as low drug loading and potential toxicity.

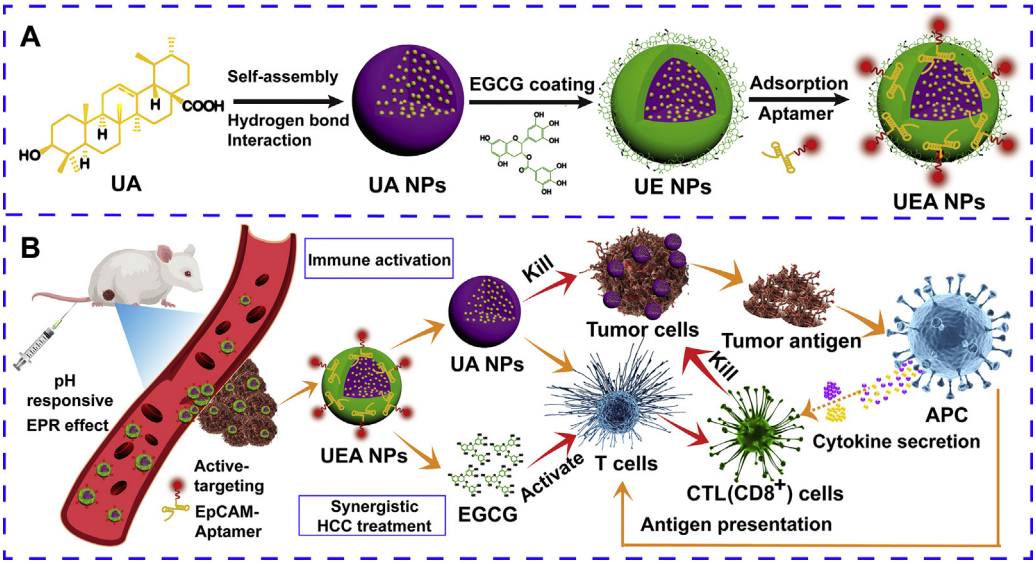

Figure 1 Schematic design and treatment of the dual-drugs co-assembly nano-delivery system. (A) The preparation of the "carrier-free" Apt-modified nanodrug based on the UA and EGCG. (B) Synergistic HCC treatment of the nanosystem by activating the innate and acquired immunity.

2. Materials and methods

2.1. *Materials*

Ursolic acid (UA), cell counting kit-8 (CCK-8), epigallocatechin gallate (EGCG), DAPI and Cy5 were bought from Aladdin Reagents Co., Ltd. (Beijing, China). The EpCAM-Apt (Apt, sequence: 5′-CACTACAGAGGTTGCGTCTGTCCCACGTTGT CATGGGGGGTTGGCCTG-3′) was purchased from Sangon Biotech Co., Ltd. (Shanghai, China). All the other solvents were obtained from domestic suppliers and used in accordance with product instructions.

2.2. *Preparation of UA NPs*

UA NPs were prepared by a solvent exchange method follows our previously protocol. Briefly, 4.57 mg UA powder was first dissolved in methanol to gain a final concentration of 1 mmol/L UA/methanol solution. Then 100 μL of the solution was dropped into 900 μL water slowly at room temperature under vigorous stirring at 1000 rpm (Eppendorf, 5424R, Hamburg, Germany). The mixture was exposed to ultrasound (500 W, 40 kHz) for 20 min, and methanol was evaporated under nitrogen. This solution was centrifuged at 3000 rpm for 10 min (Eppendorf), and the precipitate was discarded to get the UA NPs solution.

2.3. *Surface modification of UA NPs with EGCG and Apt*

Different concentrations (20%, 15%, 10% and 5%) of EGCG solution were prepared in water and then added to UA NPs solution at pH 7.8. The mixture was stirred at 1000 rpm for 10 min (Eppendorf) to get EGCG coated UA nanoparticles (UA@EGCG NPs, UE NPs). After that, 10 μL of the EpCAM-aptamer (10 mmol/L) was dropped into 990 μL of UE NPs solution and stirred at 500 rpm overnight to obtain UA@EGCG-Apt NPs (Kebai, ZHWY-200B, Guangzhou, China).

2.4. *Characterization of UA@EGCG-Apt NPs (UEA NPs)*

Mean size and zeta potential of the obtain product was determined by dynamic light scattering (DLS, Malvern panalytical, Nano-S90, Malvern, UK) to study the size distribution of nanoparticles. The morphology of nanoparticles were characterized by scanning electron microscope (SEM, FEI, Verios G4 UC, Hillsborough, Oregon, USA), transmission electron microscopic (TEM, Tecnai G2F20) and atomic force microscopy (AFM, Bruker, Nano Surface Division, Madison, Wisconsin, USA) in order to investigate physical characteristics of the synthesized nanoparticles. Sample preparation methods were similar to the previous reports. To testify whether Apt was successfully attached to UE NPs, a 12% polyacrylamide gel electrophoresis (PAGE) was employed accompanied by SYBR green as a fluorescent indicator, and the image was captured *via* bio-Rad Imager System (Bio-rad, GelDoc XR+, Berkeley, California, USA). The Apt encapsulation efficiency was evaluated by measuring the amount of unloaded free Apt in the supernatant of the solution as in Eq. (1):

$$\text{Graft rate } (\%) = W_T/(W_T + W_F) \times 100 \quad (1)$$

where W_T is the total weight of Apt and W_F is the weight of free Apt.

2.5. *Drug loading and drug release profile*

Drug loading was calculated by the weight ratio of the encapsulated drugs to the entire drug-loaded nanoparticles. The UE NPs solution was centrifuged for 10 min at 1500 rpm (Eppendorf 5424R, Hamburg, Germany). After that, 20 μL of the supernatant was diluted in 180 μL of methanol (1:9, *v*/*v*), and the concentration of the UA in UE NPs was determined by UV−Vis measurement at about 210 nm (Shimadzu, UV2700, Kyoto, Japan).

In vitro drug release studies of nanocomplex were performed using the dialysis membrane method[38]. 1 mL UA, UA and UE

NPs solution were sealed in dialysis bags (Sigma, 1000 MW cut off, Saint Louis, Missouri, USA), respectively. Then immersed the bags into beakers with 200 mL of the PBS solution (pH 7.4 or 5.5) containing 0.1% (*v*/*v*) Tween 80. After that, the beakers were placed into a water bath at 37 °C, stirring at the speed of 100 rpm for 48 h (Kebai). Samples were withdrawn at certain time intervals (0.5, 1, 2, 4, 8, 12, 24 and 48 h), and UV−Vis was used to analyzed drug content of the samples.

2.6. *The stability of the NPs and the hemolysis assay*

The particles size of prepared NPs (dissolved in water) was detected by DLS in different time points with stored at RT. Meanwhile, the same process was performed after the NPs dispersed in PBS, normal saline (NS), DMEM, DMEM+10% FBS. In addition, the particles size of NPs dispersed in mice plasma at different time points were also tested to investigate the stability of NPs in physiological environment.

The fresh blood was obtained from healthy mice to isolate the red blood cells (RBCs), with centrifugation at 2500×*g* for 5 min and washed by PBS for three times (Eppendorf). The 2% RBCs re-suspension was prepared with PBS, and 0.5 mL suspension incubated with 0.5 mL NPs (dissolved in PBS) at 37 °C for 3 h, followed by centrifugation at 2500×*g* for 5 min (Shimadzu). The OD value of different groups was tested at 504 nm, and the hemolysis ratio was measured compared to the negative control of PBS and positive control of water. More than 5% indicated a hemolytic effect.

2.7. *In vitro cellular uptake of UEA NPs*

HepG2 and HeLa cells were seeded in a 24-well plate (~1 × 10^5 cells per well) with a clean coverslip was put in each well beforehand. To prepare the Cy5-labeled NPs, the UA NPs, UE and UEA NPs solution (UA, 1 mmol/L) were poured into 10 mL of water respectively, which contained 80 μg of Cy5, at room temperature under vigorous stirring at 1000 rpm (Kebai). After being mixed for 10 min, an ultrasound was performed on the sample for 15 min. Finally, the solution was purified by water with a dialysis membrane (MWCO 1000) over 24 h, and then the dialysate was dried by lyophilization to yield Cy5-labeled NPs. The fluorescence scanning from 625 to 695 nm was performed to prove the efficient conjugation of Cy5 to the NPs with the control of free Cy5. After the incubation of the cells for 24 h, the plate was washed twice with PBS, and the cells were treated with 100 μL of fresh medium containing different of NPs groups (UA, 8 μg/mL), respectively. Four hours later, cells were washed three times with ice-cold PBS. Then DAPI was used to stain the nucleus for 15 min, and images were acquired using a confocal laser scanning microscope (CLSM) and main fluorescence intensity were measured by flow cytometry.

2.8. *Cytotoxicity assay*

The cytotoxicity effect of EGCG, UA, UA NPs, UE and UEA NPs was examined by CCK-8 assay. Firstly, the cells were seeded in a 96-well plate (~1 × 10^4 cells per well) and incubated for 24 h. Secondly, cells were treated with 100 μL fresh medium containing various concentrations (UA: 0, 1, 10, 20, 30, and 50 μmol/L) for 24 h. Untreated cells in the same plate were used as the blank control. Subsequently, the culture medium was replaced by 100 μL of CCK8 solution and incubated for another 4 h. Finally, the absorbance of each well was measured at 450 nm using a microplate reader. The combination index (CI) of UA NPs and EGCG in co-assembly UE NPs was calculated according to Eq. (2):

$$CI = DA/DmA + DB/DmB \quad (2)$$

where DA and DB were the concentrations of UA NPs and EGCG, respectively, that in UE NPs produced a certain level of

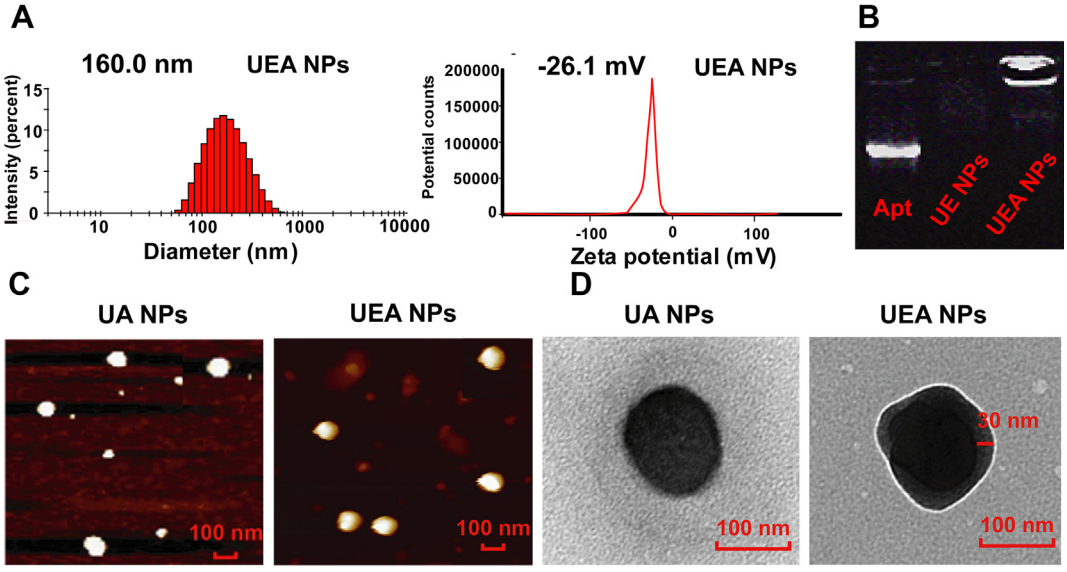

Figure 2 Characterization of prepared co-assembly NPs. (A) Mean sizes and zeta potential of UEA NPs. (B) Polyacrylamide gel electrophoresis of Apt, UE and UEA NPs to make sure the conjugation of Apt to NPs. (C)–(D) AFM and TEM images of UA and UEA NPs.

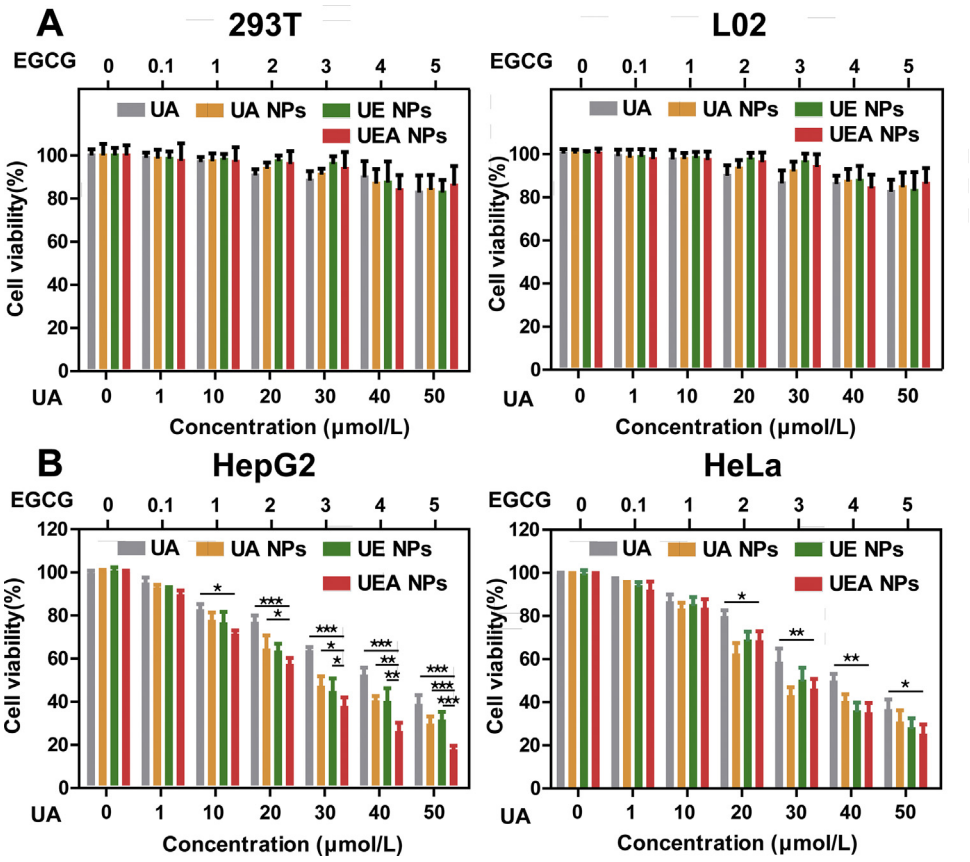

Figure 3 Cytotoxicity assay of UA and NPs in cancerous cells and noncancerous cells. Inhibitory effects on (A) HEK293T, L02 cells and (B) HepG2, HeLa cells after incubated with different concentrations of UA, UA NPs, UE NPs, and UEA NPs for 24 h. Data are presented as mean ± SD ($n = 6$); $^{*}P < 0.05$; $^{**}P < 0.01$; $^{***}P < 0.001$.

cytotoxicity. DmA and DmB were the concentrations of the free UA NPs and free EGCG that produced the same effect.

2.9. *In vivo anti-tumor effects of UEA NPs*

All animal studies were performed according to National Natural Science Foundation of China regulation and permitted by Ethics Committee for Experimental Animals of Fuzhou University (Fuzhou, China). Six-week-old male KM mice were purchased from Shanghai Laboratory Animal Center (Shanghai, China). Animals were treated with each formulation after tumor volumes reached 50 mm^3. Thirty KM mice were randomly divided into six groups: (a) wild type mice treated with normal saline group (WT), (b) tumor-bearing mice treated with 0.9% normal saline group (NS), (c) free UA group, (d) UA NPs group, (e) UE group, and (f) UEA group. Each formulation was injected six times at 3-day intervals with an equivalent UA dose of 4 mg/kg and EGCG dose of 0.4 mg/kg *via* tail vein. Meanwhile, body weights of mice and tumor volume were measured every day. Cy5-labeled NPs were used for the *in vivo* imaging. Fluorescence imaging were acquired by Caplier IVIS Lumina at 0.5, 2, 6, 12 and 24 h after intravenous injection, the tumor and major organs were dissected and washed with 0.9% normal saline to obtain the fluorescence images. The tumor tissues were harvested for weighing and tissue slice (heart, liver, spleen, lung and kidney) were detected by hematoxylin-eosin (HE) staining.

2.10. *Synergistic immune activated effects of UEA NPs*

Peripheral blood mononuclear cell (PBMCs) of mice was collected by Ficoll gradient separation[39]. The mRNA expression of cytokines was investigated by qRT-PCR after treated with different of NPs. *In vivo* experiment, the percentage of $CD4^+$ and $CD8^+$ T cells of blood, and $CD8^+$ T cells of tumor tissue suspension were calculated by flow cytometry. The WT group and NS group were used as negative and positive control. Afterwards, the serum was acquired after centrifugation at 1000 rpm for 10 min (Eppendorf). The concentration of cytokines (IL-12 and IFN-γ) was measured by enzyme-linked immunosorbent assay (ELISA) kit.

2.11. *Statistical analysis*

All *in vitro* experiments were performed at least three times and the acquired are presented as mean ± standard deviation (SD). The *t*-test was performed to analyze the data significance. $^{*}P < 0.05$, $^{**}P < 0.01$, $^{***}P < 0.001$ were considered significant. *In* experiment *in vivo*, two-way ANOVA was used to analyze the difference between treatment groups and control or the UEA NPs

and the other groups. $^{*}P < 0.05$, $^{**}P < 0.01$, and $^{***}P < 0.001$ were considered significant. All computations were made by SPSS statistical software (IBM, Amonk, NY, USA).

3. Result and discussion

3.1. Construction and characterization of UA@EGCG-Apt NPs

The construction of the nanosystem was shown in Fig. 2, UA@EGCG-Apt NPs (UEA NPs) was fabricated *via* first simply self-assembly to form UA NPs, EGCG was then coated in the surface of UA NPs to shape a core–shell structure, ending up with EpCAM-aptamer (Apt) modification. The nanocomplex was optimized through applying different molar ratios between UA and EGCG, and then characterizing them with the measurement of the drug loading efficiency and the mean particles size. As shown in Supporting Information Table S1, particle size of UA@EGCG NPs (UE NPs) irregularly changed with the variation of the ratio. The best molar ratio of 10/1 between UA and EGCG was chosen for the high drug loading efficiency of UA and the smaller particles size. The possible interactions between UA and EGCG are shown in Supporting Information Fig. S1, mainly *via* hydrophobic interactions (in purple) and hydrogen bond interactions (in green). The particles size of UA NPs changed from 123.6 to 137.0 nm (UE NPs) with EGCG coating. SEM images show the UA and UE NPs displayed spherical shapes and indicated a close agreement with measured date (Supporting Information Fig. S2).

Subsequently, the Apt was binding on the surface of UE NPs through adsorption of EGCG to nucleic acid. UEA NPs were prepared according to the result of particles size and encapsulation efficiency of Apt by optimization of molar ratio (Supporting Information Table S2). With the good particles size of 160.0 nm and zeta potential of −26.1 mV (Fig. 2A), UEA NPs got the high Apt encapsulation efficiency of 85.2% and the amount of Apt was about 410.4 nmol/mg by centrifugal assay. To prove the significant binding of Apt, the outcome of PAGE in Fig. 2B shows that free Apt is seen in lane 1, whereas the UEA NPs does not show any stripe ascribe to their high molecular weight (lane 3), suggesting that Apt were successfully absorbed onto the surface of self-assembly nanosystem. The further electrophoresis assay also proved the effective conjugation of Apt at molar ratio of 10:1:1 (Supporting Information Fig. S3). Additionally, AFM images show the similar particle size of UEA NPs (Fig. 2C), and the TEM images provided direct evidence for the formation of coatings of UEA NPs compared the UA NPs (Fig. 2D, and enlarged view of Supporting Information Fig. S4), which explained the successful construction of core–shell structure. The particles size and zeta potential of prepared UA, UE and UEA NPs are shown in Supporting Information Fig. S5.

3.2. Stability and drug release of UEA NPs

To verify stability of self-assembly nanoparticles, UA, UE and UEA NPs in water solution were left at room temperature and measured at different time points. In dynamic light scatting (DLS) measurement, the average diameter of UE and UEA NPs had no significant changes in both of the size, while UA NPs was changed from 123.6 to 216.3 nm in 14 days (Supporting Information Fig. S6). In addition, we used the more different solvents to evaluate the stability of the NPs in PBS, 0.9% normal saline, DMEM and DMEM+10% FBS (Supporting Information Fig. S7). The results prove the good stability of UE and UEA NPs under the different of the media compared with the UA NPs, indicating the stable "shell" of EGCG coating. Moreover, the good stability of UE and UEA NPs in plasma was proved compared with the UA NPs. By checking the change of particles size of UE and UEA

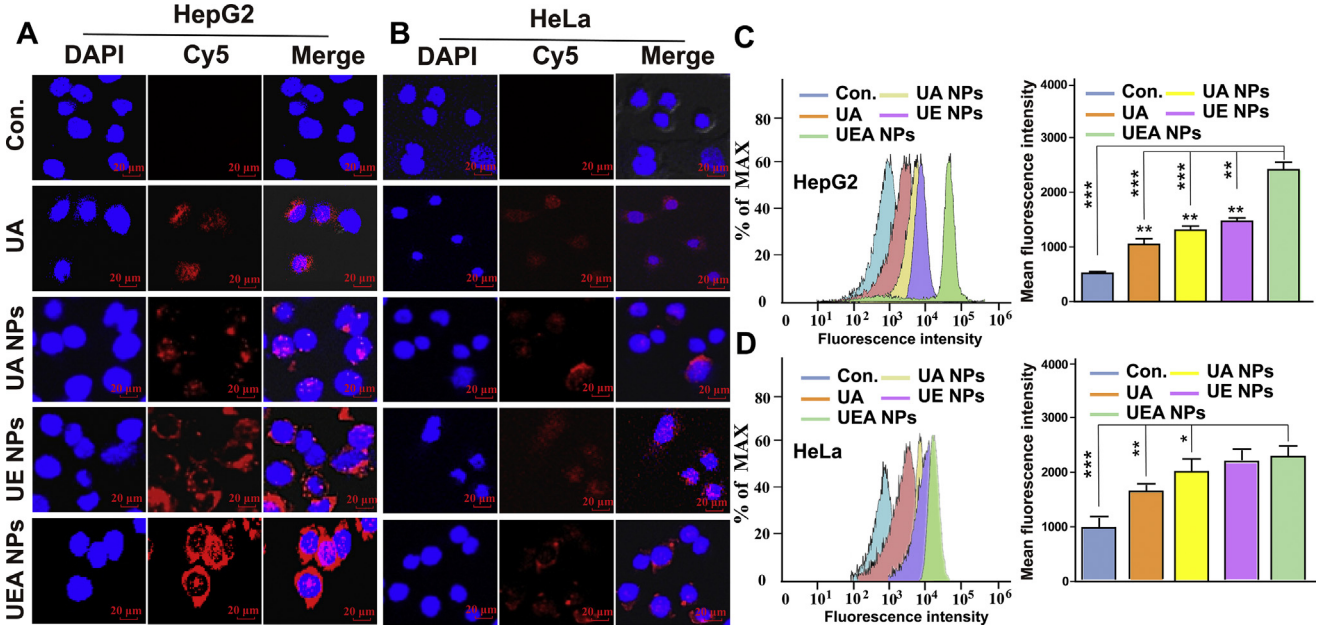

Figure 4 Cellular uptake of UEA NPs in HepG2 cells and HeLa cells. Confocal images of HepG2 cells (A) and HeLa (B) incubated with UA, UA NPs, UE NPs and UEA NPs for 4 h. (C)–(D) Flow cytometry detection of cell uptake and mean fluorescence intensity of HepG2 and HeLa cells after incubation with different formulations. Data are presented as mean ± SD ($n = 3$); $^{*}P < 0.05$; $^{**}P < 0.01$; $^{***}P < 0.001$.

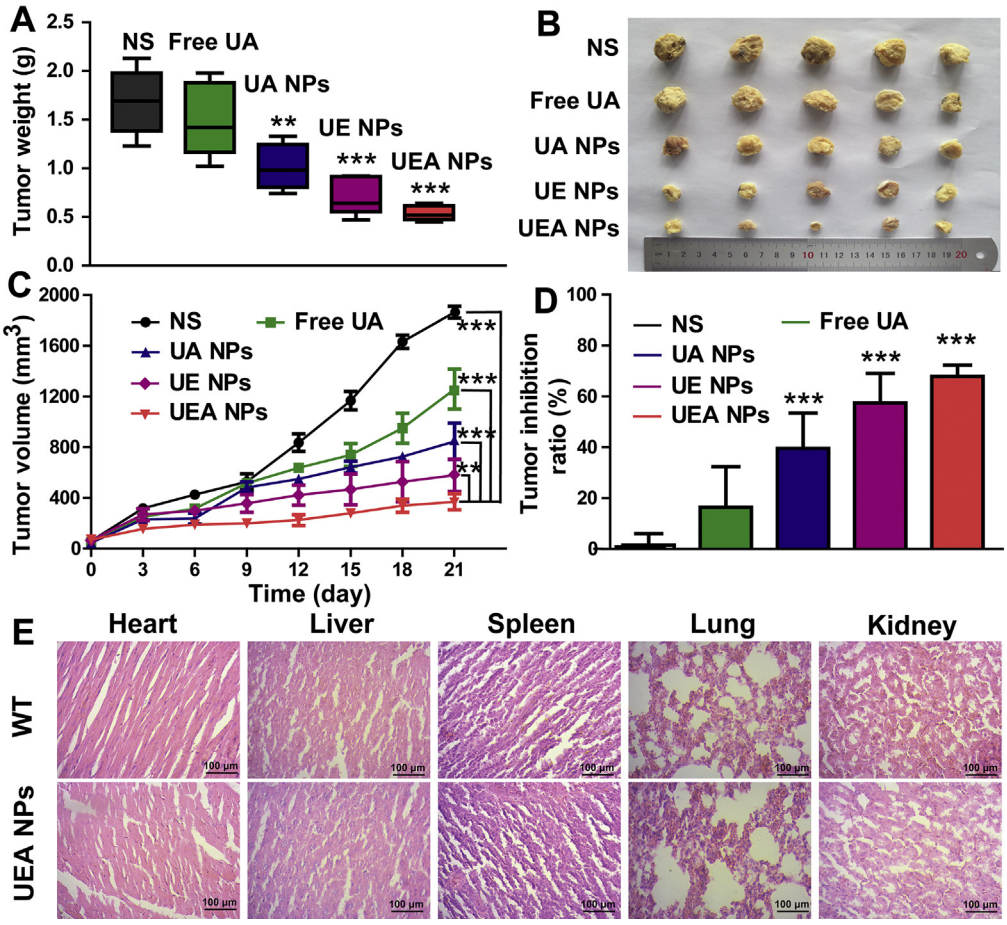

Figure 5 Investigation of *in vivo* antitumor effect of the nanosystem. (A) Tumor weight excised from mice after different formulations of treatment at 21 days. $^{*}P < 0.05$, $^{**}P < 0.01$, $^{***}P < 0.001$ significant in comparison to the NS control group. (B) Image of tumor tissues separated from mice treated with different formulations. (C) Tumor volume growth curves after different formulations of treatment. The difference between UEA NPs and other groups were statistically significant ($^{**}P < 0.01$, $^{***}P < 0.001$). (D) Tumor inhibition ratio of different formulations in HCC treatment. $^{***}P < 0.001$ significant in comparison to the NS control. (E) HE staining of heart, liver, spleen, lung and kidney from mice of WT and UEA NPs.

NPs in plasma, we found particles size of two types of NPs presented a brief increase in 12 h and then a gradual decrease (Supporting Information Fig. S8). We hypothesized that it was due to the EGCG of NPs absorbing a certain amount of plasma protein to make itself stable in the blood. Afterwards, EGCG would gradually depolymerize and caused the decreased particles size. The result shows that EGCG coating improved the stability of self-assembly NPs.

To investigate pH-responsive manner of UA release from UE NPs, we conducted *in vitro* drug release assay under pH 5.5 or pH 7.4 over 48 h at 37 °C. As is shown in Supporting Information Fig. S9, the release percentage of UA from UE NPs is approximately 70% at pH 5.5, while drug release percentage is below 50% at pH 7.4, suggesting its pH-dependent manner. Similar result appeared in UA NPs, the release percentage of UA at pH 5.5 was much more abundant than free UA. In view of the release profile, UE NPs were stable in normal extracellular environment, however, it released rapidly in weak acid condition, where tumor cells live in.

3.3. *Cytotoxicity assay*

The cytotoxicity effect of nanosystem was examined by CCK-8 assay. In order to avoid side effects in biological systems, the absence of toxicity in normal tissues is a desirable property. At first, the self-assembly nanosystem was investigated in noncancerous HEK293T cells and normal L02 liver cells (Fig. 3A). There was no significant inhibition of cell proliferation was found in different of groups even in a large dose of 50 μmol/L (UA). The result show that the nanosystem exhibited low toxicity and good biosafety in normal cells. Subsequently, as verified in Supporting Information Fig. S10 by Western blot, EpCAM-positive HepG2 and H22 cells, EpCAM-negative HeLa cells were used in the experiment. Cytotoxic effect of UA, UA NPs, UE NPs, and UEA NPs in both HeLa and HepG2 cells displayed a dose-dependent manner. By contrast, UE and UEA NPs exhibited considerable cytotoxicity in cancerous cells compared to the free UA and UA NPs (Fig. 3B). We found that UA NPs achieved the median lethal of the HepG2 cells at about 40 μmol/L. Meanwhile, according to

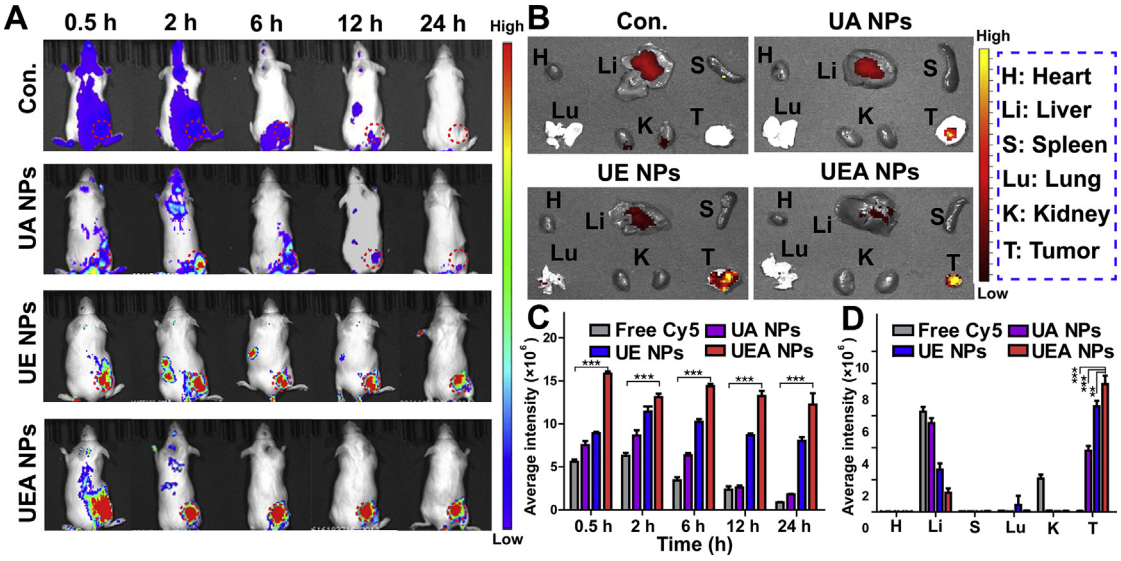

Figure 6 *In vivo* fluorescence imaging of free Cy5 and different of NPs. (A) Fluorescence images of HCC model mice injected with three NPs recorded at 0.5, 2, 6, 12, and 24 h with the free Cy5 as control. (B) Fluorescence images of the major organs and tumors of HCC model mice injected with free Cy5 and NPs. (C)–(D) The average fluorescence intensity of tumor site at different time points, the major organs and tumors of different groups. Values represented are the mean ± SD. $^{**}P < 0.01$, $^{***}P < 0.001$.

the cytotoxicity of free EGCG on HepG2 cells as shown in Supporting Information Fig. S11, EGCG killed only 10 percent of the cells at the same concentration. Although UA was mainly responsible for tumor cell killing according to the IC50 of results, EGCG also enhances the cytotoxicity of the nanosystem formed by co-assembly. The combination index (CI) of UE NPs < 1 revealed that the co-assembly of UA and EGCG at the molar ratio of 10:1 was acting synergistically instead of the additive effect or antagonistic (Supporting Information Fig. S12).

It is worth noting that higher change of cytotoxicity was displayed between UE and UEA NPs in HepG2 cells rather than HeLa cells, indicating that UEA NPs enabled to target EpCAM-positive HCC cells. In addition, the similar result was proved in H22 cells as shown in Supporting Information Fig. S13, UEA NPs significantly increased cytotoxicity of nanodrug in EpCAM-positive cells compared to the other NPs and free UA. The results might be caused by the better cellular uptake of UEA NPs with Apt modification so as to induce the higher cytotoxicity.

3.4. *In vitro cellular uptake of UEA NPs*

To explore cellular uptake of UEA NPs in HepG2 and HeLa cells, DAPI was used to stain nuclei (shown in blue), Cy5 was used to locate the NPs (shown in red). Firstly, the same characteristic fluorescence absorption peak were detected in the NPs after the Cy5 incubation, which proved that the successful labeling of the Cy5 on the NPs (Supporting Information Fig. S14). Afterwards, as shown in Fig. 4A, when HepG2 cells were treated with each formulation, cells could be seen surrounding by red color, and the fluorescence intensity of UEA NPs group was obviously stronger than UA NPs, UE NPs and free UA groups. However, there was no distinct fluorescence was seen and no significant shift was observed for EpCAM-negative HeLa cells in different groups (Fig. 4B). This result demonstrate that UEA NPs could improve cellular uptake of drugs in EpCAM-positive cells, and the addition of Apt might be responsible for cellular uptake reinforcement of UEA NPs. Flow cytometry analysis also revealed that the obvious increase of cellular uptake of UEA NPs in HepG2, while there was no significant change between UEA and UE NPs in HeLa cells (Fig. 4C and D). These data further confirm that Apt modification improved intracellular uptake of nanoparticles in EpCAM-positive HCC cells.

3.5. *In vivo anti-tumor effects of UEA NPs*

In vivo HCC treatment efficiency of UEA NPs was investigated by tumor-bearing mice. H22 cells were injected into the right posterior limb of the male KM mice to establish xenograft tumor models. During the period of treatment, the tumor-bearing mice and wild type mice treated with normal saline were performed as the positive control group (NS) and the negative control group (WT). When it comes to tumor growth, the free EGCG exhibited the weak therapeutic effect (Supporting Information Fig. S15). Although the tumor inhibition of free UA was stronger than that of EGCG, it was still significantly lower than that of the NPs groups. Meanwhile, UA NPs, UE and UEA NPs displayed different inhibitory effects according to the weight and volume of tumors (Fig. 5A–C). It was obvious that UEA NPs could remarkably suppress tumor growth compared with the others as shown in Fig. 5D, UEA NPs got the best tumor inhibition ratio. In addition, the body weight of mice treated with UA NPs, UE and UEA NPs had no significant change compared with WT group, and significantly heavier than the tumor-bearing mice, indicating that the nanodrugs had no significant toxicity to mice (Supporting

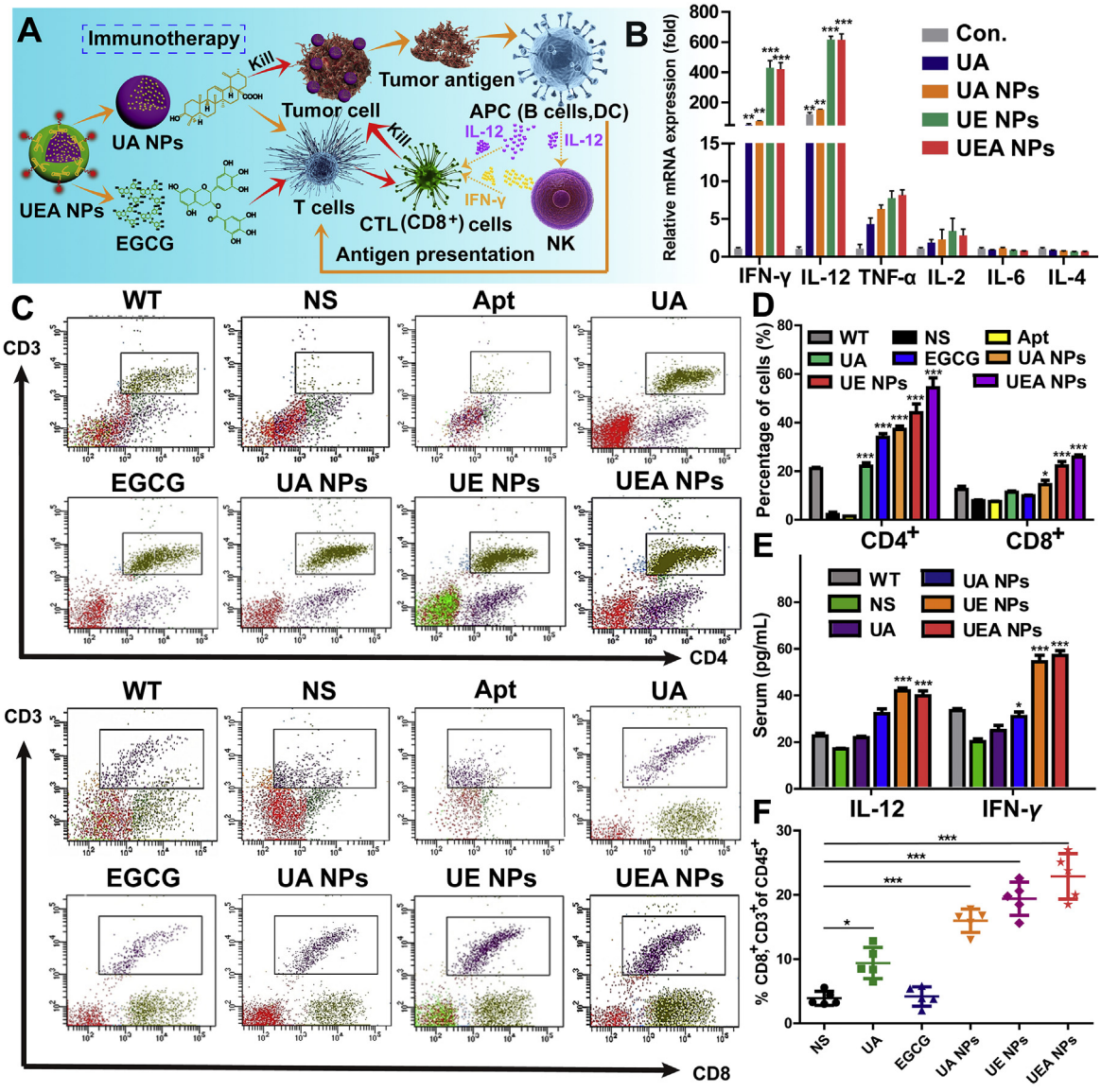

Figure 7 Assessment of immunity activation of co-assembly UEA NPs. (A) Schematic illustration of the induced immunotherapy of UA and EGCG in UEA NPs. (B) Relative mRNA expression of cytokines secretion in mouse PBMC after treated with UA, UA NPs, UE NPs, UEA NPs at the same concentration. $^{**}P < 0.01$, $^{***}P < 0.001$ significant in comparison to the control. (C)–(D) Effect of UA, EGCG, Apt and NPs groups on expression of $CD4^+$ and $CD8^+$ T cells *in vivo*. $^{*}P < 0.05$; $^{***}P < 0.001$ significant in comparison to the NS group. (E) Serum IL-12 and IFN-γ levels post intravenous administration of 0.9% saline, UA NPs, UE NPs or UEA NPs. $^{*}P < 0.05$; $^{***}P < 0.001$ significant in comparison to the NS group. (F) Tumor-infiltrating $CD8^+$ T cells from tumor tissues. Data are presented as mean ± SD ($n = 5$); $^{*}P < 0.05$; $^{***}P < 0.001$.

Information Fig. S16). To further investigate the biosafety of the nanocomplex, hemolysis assay was performed by mixing the red blood cells and the NPs with the same concentration using *in vivo* (Supporting Information Fig. S17). With the water and PBS used as the control, the hemolysis ratio of UEA NPs were less than 5%, which showed the nanoparticles had no hemolysis effect to damage red blood cells. However, we found that the hemolysis ratio was increased in UE and UEA NPs compared to the UA NPs after the EGCG coating. Hence, we further explored the hemolysis effect of free EGCG, and the result revealed that EGCG induced the erythrocyte hemolysis at about 1 mg/mL. The nanodrug was safe due to the concentration of EGCG in UEA NPs used in treatment was about 0.1 mg/mL. In addition, no evidence of toxicity was observed on heart, liver, spleen, lung and kidney after treatment with UEA NPs compared to the WT group by hematoxylin-eosin (HE) staining (Fig. 5E), indicating good biocompatibility of the co-assembly nanosystem *in vivo*.

In vivo fluorescence imaging was used to visualize the tumor accumulation ability of NPs. As shown in Fig. 6A, fluorescence imaging exhibited an obvious tumor accumulation of three types of NPs after 24 h treatment by i.v. injection compared to the control group of free Cy5. The average quantitative fluorescence intensity of NPs in the tumor sites was higher than control group at different time points. Meanwhile, we found that the UEA and UE NPs increased the long circulation of the nanodrug in the body. The obvious nanodrug accumulation at tumor site in UE and

UEA NPs groups could be found after 24 h, while no UA NPs accumulation was observed after 12 h. The result proves the good property of the "shell" of EGCG in long circulation and efficient release in tumor microenvironment. In addition, the efficient tumor tarting of Apt was verified for that the UEA NPs got the higher tumor accumulation that UE NPs by the measurement of average intensity (Fig. 6C). The tumor and major organs distribution of drugs also showed that the UEA NPs significantly booted the tumor accumulation of nanodrugs (Fig. 6B and D). The results indicate that novel nanoparticles had the effective targeting to tumor and enhanced the tumor accumulation.

3.6. Assessment of synergistic immune response effects of UEA NPs

The favorable performance of UEA NPs in inhibiting tumor growth has been demonstrated above, and its mechanism by immune activation was thus investigated (Fig. 7A). In case of influence from other immune stimulants, we investigated that there was no impurity, like lipopolysaccharide (LPS), existing in the solution except for the UA, EGCG and Apt, as proved in Supporting Information Fig. S18. We first extracted the tumor-bearing mouse peripheral blood mononuclear cells (PBMCs) and treated them with different of formulation as *in vivo* experiment. PBMCs was mainly composed of monocytes and lymphocytes, which included T cells, B cells and NK cells. IL-12 was secreted mainly by B cells and played an important role in stimulating the expression of IFN-γ by activating NK cells. The several of primary cytokines secreted by PBMCs were evaluated on the mRNA expression level (Fig. 7B, and Supporting Information Fig. S19). The result found that the IL-12 and IFN-γ were significantly activated with UEA NPs incubation, and the innate immune activation of NK cells was confirmed. Meanwhile, IL-12 and IFN-γ were involved in the activation and maturation of T cells. Subsequently, blood of mice from drug treatment groups was collected in the experiment for the further investigation. This result shows that the immune system of tumor-bearing mice (NS group) was strongly inhibited by the tumor. There were UA and EGCG in nanocomplex playing the important roles in immune activation of T cells, and Apt had no immune stimulatory properties. Both of the percentage of $CD4^+$ and $CD8^+$ T cells from the UE and UEA NPs group remarkable increased compared with the free drugs-treated mice and tumor-bearing mice, and UEA NPs exhibited more efficient immunotherapy than UE NPs due to the better tumor accumulation with the Apt modification (Fig. 7C and D). Typically, the ratio of $CD4^+/CD8^+$ ranges from 1.4 to 2.0, as for tumor-bearing group, the ratio was lower than the normal range, while for the UEA NPs group, the ratio was significantly higher than the normal value, indicating an immune-enhancing effect of NPs (Supporting Information Fig. S20). The increased expression of IL-12 and IFN-γ in serum was also proved by ELISA assay, which was consisted with the result of PBMCs *in vitro* (Fig. 7E). It is noteworthy that the increased cytokines such as TNF-α, IL-12 and IFN-γ were mostly secreted by Th1 cells in PBMCs, which was an important evidence for improvement of Th1/Th2 imbalance in cancer. The result above confirms what we hypothesized before, the self-assembly dual-nanodrug induced the cells death to provide the tumor antigen on the one hand, and activated the secretion of IL-12, IFN-γ of antigen-presenting cells and NK cells in innate immunity on the other hand. Finally, the activation of acquired immunity achieved the further clearance of tumor, UEA NPs significant enhanced the tumor immune infiltration that large amount of the CTL ($CD8^+$ T cells) was detected in the tumor tissues (Fig. 7F and Supporting Information Fig. S21). Overall, UEA NPs showed the efficient immunotherapy for HCC treatment.

4. Conclusions

In this study, we demonstrate that EpCAM-aptamer functionalized UA NPs coated with EGCG induced potent anti-tumor effect *in vitro* and *in vivo via* activating immunity of the organism. The nanosystem exhibited robust stability, pH-responsive, synergistic effect in cytotoxicity and more efficient HCC cellular uptake than UA NPs or insoluble UA through EpCAM activate targeting. *In vivo* fluorescence imaging showed the effective tumor accumulation and long circulation of UEA NPs. Moreover, UEA NPs achieved higher immunostimulatory efficacy, as shown in IL-12 and IFN-γ secretion, activation of $CD4^+$ and $CD8^+$ T cells and the immune infiltration in tumor tissues, suggesting that the modification of aptamer further enhanced synergistic effect of the dual-drugs treatment. Furthermore, we found that the systemic delivery of UEA NPs resulted in a "green" and safe therapy through monitoring body weight and HE staining of tumor-bearing mice. Taken together, the preparation of UEA NPs was a promising strategy for combining co-assembly nanoscale natural products, thereby exerting synergistic induction of immunotherapy, against HCC in future clinical trials.

Acknowledgments

This project was supported by the National Natural Science Foundation of China (81972832), Natural Science Foundation of Fujian Province (2018J01895, China) and College Students' Innovation and Entrepreneurship Training Program of Fujian Province (S202010386051, China).

Author contributions

Bingchen Zhang, Jiali Jiang and Jingwei Shao designed the research. Pengyu Wu and Junjie Zou carried out the experiments and performed data analysis. Juanfang Lin, Chao Li, Bangyue Luo, and Yongjie Zhang participated part of the experiments. Jingqing Le and Rui Huang provided experimental drugs and quality control. Bingchen Zhang and Jiali Jiang wrote the manuscript. Jingwei Shao revised the manuscript. All of the authors have read and approved the final manuscript.

Conflicts of interest

The authors have no conflicts of interest to declare.

Appendix A. Supporting information

Supporting data to this article can be found online at https://doi.org/10.1016/j.apsb.2020.07.026.

References

1. Chen SZ, Cao QQ, Wen W, Wang HY. Targeted therapy for hepatocellular carcinoma: challenges and opportunities. *Canc Lett* 2019;**460**:1−9.
2. Sia D, Villanueva A, Friedman SL, Llovet JM. Liver cancer cell of origin, molecular class, and effects on patient prognosis. *Gastroenterology* 2017;**152**:745−61.
3. Ghosh D, Choudhury ST, Ghosh S, Mandal AK, Sarkar S, Ghosh A, et al. Nanocapsulated curcumin: oral chemopreventive formulation against diethylnitrosamine induced hepatocellular carcinoma in rat. *Chem Biol Interact* 2012;**195**:206−14.
4. Asghar U, Meyer T. Are there opportunities for chemotherapy in the treatment of hepatocellular cancer?. *J Hepatol* 2012;**56**:686−95.
5. Zhang WX, Zhang ZZ, Zhang YG. The application of carbon nanotubes in target drug delivery systems for cancer therapies. *Nanoscale Res Lett* 2011;**6**:555.
6. Gynther M, Proietti SI, Hansen JC, Hansen KB, Malm T, Ishchenko Y, et al. Augmentation of anticancer drug efficacy in murine hepatocellular carcinoma cells by a peripherally acting competitive *N*-methyl-D-aspartate (NMDA) receptor antagonist. *J Med Chem* 2017;**60**:9885−904.
7. Li C, Wang JC, Wang YG, Gao HL, Wei G, Huang YZ, et al. Recent progress in drug delivery. *Acta Pharm Sin B* 2019;**9**:1145−62.
8. Shanmugam MK, Nguyen AH, Kumar AP, Tan BK, Sethi G. Targeted inhibition of tumor proliferation, survival, and metastasis by pentacyclic triterpenoids: potential role in prevention and therapy of cancer. *Canc Lett* 2012;**320**:158−70.
9. Kashyap D, Tuli HS, Sharma AK. Ursolic acid (UA): a metabolite with promising therapeutic potential. *Life Sci* 2016;**146**:201−13.
10. Yin R, Li T, Tian JX, Xi P, Liu RH. Ursolic acid, a potential anticancer compound for breast cancer therapy. *Crit Rev Food Sci Nutr* 2018;**58**:568−74.
11. Guo Y, Jiang K, Shen ZC, Zheng GR, Fan LL, Zhao RR, et al. A small molecule nanodrug by self-assembly of dual anticancer drugs and photosensitizer for synergistic near-infrared cancer theranostics. *ACS Appl Mater Interfaces* 2017;**9**:43508−19.
12. Jiang K, Chi T, Li T, Zheng GR, Fan LL, Liu YJ, et al. A smart pH-responsive nano-carrier as a drug delivery system for the targeted delivery of ursolic acid: suppresses cancer growth and metastasis by modulating P53/MMP-9/PTEN/CD44 mediated multiple signaling pathways. *Nanoscale* 2017;**9**:9428−39.
13. Wang ML, Zhao TT, Liu YP, Wang QQ, Xing SS, Li L, et al. Ursolic acid liposomes with chitosan modification: promising antitumor drug delivery and efficacy. *Mater Sci Eng C Mater Biol Appl* 2017;**71**:1231−40.
14. Shen ZC, Li BW, Liu YJ, Zheng GR, Guo Y, Zhao RR, et al. A self-assembly nanodrug delivery system based on amphiphilic low generations of PAMAM dendrimers–ursolic acid conjugate modified by lactobionic acid for HCC targeting therapy. *Nanomedicine* 2018;**14**:227−36.
15. Liu G, Gao JH, Ai H, Chen XY. Applications and potential toxicity of magnetic iron oxide nanoparticles. *Small* 2013;**9**:1533−45.
16. Zhao YY, Chen F, Pan YM, Li ZP, Xue XD, Okeke CI, et al. Nanodrug formed by coassembly of dual anticancer drugs to inhibit cancer cell drug resistance. *ACS Appl Mater Interfaces* 2015;**7**:19295−305.
17. Fan LL, Zhang BC, Xu AX, Shen ZC, Guo Y, Zhao RR, et al. Carrier-free, pure nanodrug formed by the self-assembly of an anticancer drug for cancer immune Therapy. *Mol Pharm* 2018;**15**:2466−78.
18. Li C, Lin JF, Wu PY, Zhao RR, Zou JJ, Zhou M, et al. Small molecule nanodrug assembled of dual-anticancer drug conjugate for synergetic cancer metastasis therapy. *Bioconjugate Chem* 2018;**29**:3495−502.
19. Jiang K, Han LY, Guo Y, Zheng GR, Fan LL, Shen ZC, et al. A carrier-free dual-drug nanodelivery system functionalized with aptamer specific targeting HER2-overexpressing cancer cells. *J Mater Chem B* 2017;**5**:9121−9.
20. Zhao RR, Zheng GR, Fan LL, Shen ZC, Jiang K, Guo Y, et al. Carrier-free nanodrug by co-assembly of chemotherapeutic agent and photosensitizer for cancer imaging and chemo-photo combination therapy. *Acta Biomater* 2018;**70**:197−210.
21. Avadhani KS, Manikkath J, Tiwari M, Chandrasekhar M, Godavarthi A, Vidya SM, et al. Skin delivery of epigallocatechin-3-gallate (EGCG) and hyaluronic acid loaded nano-transfersomes for antioxidant and anti-aging effects in UV radiation induced skin damage. *Drug Deliv* 2017;**24**:61−74.
22. Mi YS, Liu X, Tian HY, Liu H, Li J, Qi GY, et al. EGCG stimulates the recruitment of brite adipocytes, suppresses adipogenesis and counteracts TNF-alpha-triggered insulin resistance in adipocytes. *Food Funct* 2018;**9**:3374−86.
23. Shirakami Y, Shimizu M, Adachi S, Sakai H, Nakagawa T, Yasuda Y, et al. (−)-Epigallocatechin gallate suppresses the growth of human hepatocellular carcinoma cells by inhibiting activation of the vascular endothelial growth factor-vascular endothelial growth factor receptor axis. *Canc Sci* 2009;**100**:1957−62.
24. Lim YC, Park HY, Hwang HS, Kang SU, Pyun JH, Lee MH, et al. (−)-Epigallocatechin-3-gallate (EGCG) inhibits HGF-induced invasion and metastasis in hypopharyngeal carcinoma cells. *Canc Lett* 2008;**271**:140−52.
25. Li J, Wu SX, Wu CC, Qiu LP, Zhu GZ, Cui C, et al. Versatile surface engineering of porous nanomaterials with bioinspired polyphenol coatings for targeted and controlled drug delivery. *Nanoscale* 2016;**8**:8600−6.
26. Sileika TS, Barrett DG, Zhang R, Lau KH, Messersmith PB. Colorless multifunctional coatings inspired by polyphenols found in tea, chocolate, and wine. *Angew Chem Int Ed Engl* 2013;**52**:10766−70.
27. Ding J, Liang TX, Min QH, Jiang LP, Zhu JJ. "Stealth and fully-laden" drug carriers: self-assembled nanogels encapsulated with epigallocatechin gallate and siRNA for drug-resistant breast cancer therapy. *ACS Appl Mater Interfaces* 2018;**10**:9938−48.
28. Xiong HJ, Yan JH, Cai SD, He QY, Peng DM, Liu ZB, et al. Cancer protein biomarker discovery based on nucleic acid aptamers. *Int J Biol Macromol* 2019;**132**:190−202.
29. Zhou JH, Rossi J. Aptamers as targeted therapeutics: current potential and challenges. *Nat Rev Drug Discov* 2017;**16**:181−202.
30. Zhu J, Huang H, Dong SW, Ge L, Zhang Y. Progress in aptamer-mediated drug delivery vehicles for cancer targeting and its implications in addressing chemotherapeutic challenges. *Theranostics* 2014;**4**:931−44.
31. Trzpis M, McLaughlin PM, de Leij LM, Harmsen MC. Epithelial cell adhesion molecule: more than a carcinoma marker and adhesion molecule. *Am J Pathol* 2007;**171**:386−95.
32. Macdonald J, Henri J, Roy K, Hays E, Bauer M, Veedu RN, et al. EpCAM immunotherapy *versus* specific targeted delivery of drugs. *Cancers* 2018;**10**:19.
33. Yamashita T, Ji J, Budhu A, Forgues M, Yang W, Wang H, et al. EpCAM-positive hepatocellular carcinoma cells are tumor-initiating cells with stem/progenitor cell features. *Gastroenterology* 2009;**136**:1012−24.
34. Kunkel SD, Elmore CJ, Bongers KS, Ebert SM, Fox DK, Dyle MC, et al. Ursolic acid increases skeletal muscle and brown fat and decreases diet-induced obesity, glucose intolerance and fatty liver disease. *PLoS One* 2012;**7**:39332.

35. Hong ZY, Xu YQ, Yin JF, Jin JC, Jiang YW, Du QZ. Improving the effectiveness of (−)-epigallocatechin gallate (EGCG) against rabbit atherosclerosis by EGCG-loaded nanoparticles prepared from chitosan and polyaspartic acid. *J Agric Food Chem* 2014;**62**:12603−9.
36. Kim YH, Won YS, Yang X, Kumazoe M, Yamashita S, Hara A, et al. Green tea catechin metabolites exert immunoregulatory effects on $CD4^+$ T cell and natural killer cell activity. *J Agric Food Chem* 2016;**64**:3591.
37. Zheng GR, Shen YL, Zhao RR, Chen F, Zhang Y, Xu AX, et al. Dual-targeting multifuntional mesoporous silica nanocarrier for codelivery of siRNA and ursolic acid to folate receptor overexpressing cancer cells. *J Agric Food Chem* 2017;**65**:6904.
38. Lin JF, Li C, Guo Y, Zou JJ, Wu PY, Liao YQ, et al. Carrier-free nanodrugs for *in vivo* NIR bioimaging and chemo-photothermal synergistic therapy. *J Mater Chem B* 2019;**7**:6914−23.
39. Corkum CP, Ings DP, Burgess C, Karwowska S, Kroll W, Michalak TI. Immune cell subsets and their gene expression profiles from human PBMC isolated by Vacutainer Cell Preparation Tube (CPT™) and standard density gradient. *BMC Immunol* 2015;**16**:48.